Smart Mater. Struct. 7 (1998) 704–719. Printed in the UK PII: S0964-1726(98)96183-3

Comparative study of damage identification algorithms applied to a bridge: I. Experiment*

Charles R Farrar† and David A Jauregui‡

† Engineering Analysis Group, MS P946, Los Alamos National Laboratory, Los Alamos, NM 87545, USA
‡ Department of Civil Engineering, University of Texas, Austin, TX, USA

Received 14 March 1997, accepted for publication 14 July 1997

Abstract. Over the past 30 years detecting damage in a structure from changes in global dynamic parameters has received considerable attention from the civil, aerospace and mechanical engineering communities. The basis for this approach to damage detection is that changes in the structure's physical properties (i.e., boundary conditions, stiffness, mass and/or damping) will, in turn, alter the dynamic characteristics (i.e., resonant frequencies, modal damping and mode shapes) of the structure. Changes in properties such as the flexibility or stiffness matrices derived from measured modal properties and changes in mode shape curvature have shown promise for locating structural damage. However, to date there has not been a study reported in the technical literature that directly compares these various methods. The experimental results reported in this paper and the results of a numerical study reported in an accompanying paper attempt to fill this void in the study of damage detection methods. Five methods for damage assessment that have been reported in the technical literature are summarized and compared using experimental modal data from an undamaged and damaged bridge. For the most severe damage case investigated, all methods can accurately locate the damage. The methods show varying levels of success when applied to less severe damage cases. This paper concludes by summarizing some areas of the damage identification process that require further study.

1. Introduction

The interest in the ability to monitor a structure and detect damage at the earliest possible stage is pervasive throughout the civil, mechanical and aerospace engineering communities. Current damage detection methods are either visual or localized experimental methods such as acoustic or ultrasonic methods, magnetic field methods, radiography, eddy-current methods and thermal field methods (Kobayashi 1987). All these experimental methods require that the vicinity of the damage is known *a priori* and that the portion of the structure being inspected is readily accessible. Subject to these limitations, these experimental methods can detect damage on or near the surface of the structure. The need for more global damage detection methods that can be applied to complex structures has led to the development of methods that examine changes in the vibration characteristics of the structure.

Global damage or fault detection, as determined by changes in the dynamic properties or response of structures, is a subject that has received considerable attention in the literature beginning approximately 30 years ago. Based on the amount of information provided regarding the damage state, these methods can be classified as providing four levels of damage detection. The four levels are (Rytter 1993):

(1) identify that damage has occurred;
(2) identify that damage has occurred and determine the location of damage;
(3) identify that damage has occurred, locate the damage and estimate its severity and
(4) identify that damage has occurred, locate the damage, estimate its severity and determine the remaining useful life of the structure.

The basic premise of the global damage detection methods that examine changes in the dynamic properties is that modal parameters, notably resonant frequencies, mode shapes and modal damping, are a function of the physical properties of the structure (mass, damping, stiffness and boundary conditions). Therefore, changes in physical properties of the structure, such as its stiffness or flexibility, will cause changes in the modal properties. A detailed summary of vibration-based damage detection methods can be found in Doebling *et al* (1996) where the general limitations and successes of these methods are discussed.

An extensive, recent survey of bridge failures in the United States since 1950 is presented by Shirole and

* Work performed under the auspices of the US Department of Energy.

0964-1726/98/050704+16$19.50

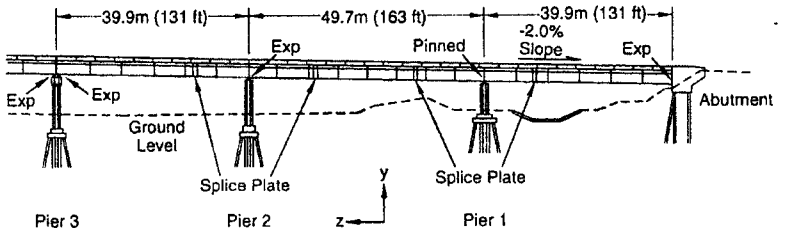

Figure 1. Elevation view of the portion of the I-40 bridge that was tested.

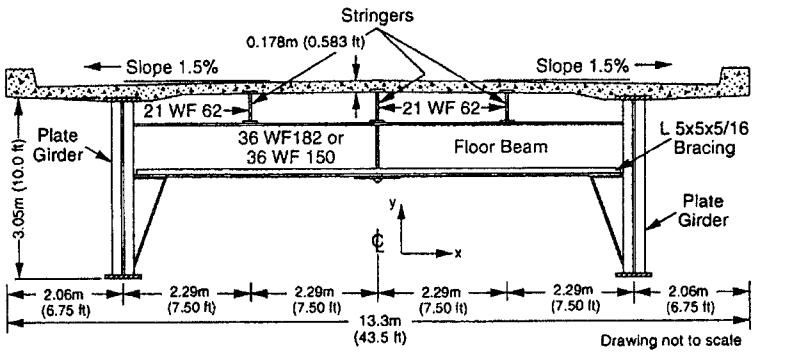

Figure 2. Cross-section geometry of the I-40 bridge.

Holt (1991). These authors point out that widespread introduction of systematic bridge inspection programs can be directly attributed to the catastrophic bridge collapse at Point Pleasant, WV, in 1967. At present, bridges are generally rated and monitored during biennial inspections, largely using visual inspection techniques that are discussed by White *et al* (1992). There is the possibility that damage could go undetected at inspection or that growth of cracks in load-carrying members to critical levels, for instance, could occur between inspection intervals (see Biswas *et al* 1990). Sudden damage leading to bridge collapse also occurs due to collision, as evidenced by the 1993 AMTRAK railroad bridge collapse in the Southeastern US involving collision of the supporting pier by a barge. Based on these findings, it appears that a quantitative, possibly continuous, mechanism of bridge damage detection is appropriate to prevent or, at least, mitigate the effects of future bridge failures. These events and the identified need for more robust damage monitoring systems have motivated investigators to study the application of global, vibration-based damage detection methods to bridge structures.

Many studies of global damage detection methods applied to bridges (e.g. see Salane *et al* 1981, Kato and Shimada 1986, Turner and Pretlove 1988, Spyrakos *et al* 1990, Mazurek and DeWolf 1990, Jian 1991, Tang and Leu 1991, Farrar *et al* 1994, Alampalli *et al* 1995) primarily examined changes in modal properties such as resonant frequencies, mode shapes and modal damping determined during measured-input and ambient vibration. These studies found that resonant frequencies and modal damping were insensitive to low levels of damage. Changes in experimentally determined mode shapes were found to be more sensitive indicators of damage. These studies also identified that changes in modal properties resulting from changes in environmental conditions can be as significant as the changes in these properties caused by damage.

Other bridge damage identification studies have examined changes in alternate vibration-based parameters including frequency response functions (FRF, the Fourier transform of the response normalized by the Fourier transform of the input) (e.g., see Biswas *et al* 1990, Samman *et al* 1991, Law *et al* 1992, Biswas *et al* 1994, Samman and Biswas 1994); mechanical impedance functions (e.g., see Salane *et al* 1981); modal assurance criterion (MAC) and coordinate modal assurance criterion (COMAC) (e.g., see Farrar *et al* 1994, Alampalli *et al* 1995, Salawu 1995, Salawu and Williams 1995); energy transfer ratios, (e.g., see Liang *et al* 1995, Kong *et al* 1995); and finite element model updating methods (e.g., see Simmermacher *et al* 1995).

Methods investigated in this study include those that examine changes in the modal strain energy (Kim and Stubbs 1993, Stubbs *et al* 1995); changes in mode shape curvature (e.g., see Pandey *et al* 1991); changes in flexibility coefficients derived from modal properties, (e.g., see Pandey and Biswas 1994), changes in stiffness coefficients derived from modal properties (e.g., see Zimmerman and Kaouk 1994); and changes in the curvature of the uniform load surface derived from modal properties (e.g., see Raghavendracher and Aktan 1992, Tokstoy and Aktan 1994 and Zhang and Aktan 1995). These methods all have the feature that they potentially are readily adapted to automated, on-line damage identification systems. However, these methods have only been applied to test structures available to the specific investigators who have developed these methods. In this study these methods

will be applied to experimental data from the same structure with the hope that the relative merits of the various methods as well as their shortcomings may be better identified and understood. An accompanying study (Farrar and Jauregui 1998) extends this comparative study using numerically simulated data.

2. Test structure geometry

The I-40 Bridges over the Rio Grande in Albuquerque, NM, razed in 1993, formerly consisted of twin spans (there are separate bridges for each traffic direction) made up of a concrete deck supported by two welded-steel plate girders and three steel stringers. Loads from the stringers are transferred to the plate girders by floor beams located at 6.1 m (20 ft) intervals. Cross-bracing is provided between the floor beams. Figure 1 shows an elevation view of the portion of the bridge that was tested. The cross-section geometry of each bridge is shown in figure 2.

Each bridge is made up of three identical sections. Except for the common pier located at the end of each section, the sections are structurally independent. A section has three spans; the end spans are of equal length, approximately 39.9 m (131 ft), and the center span is approximately 49.4 m (163 ft) long. Five plate girders are connected with four bolted splices to form a continuous beam over the three spans. The portions of the plate girders over the piers have increased flange dimensions, compared with the mid-span portions, to resist the higher bending stresses at these locations. Connections that allow for thermal expansion as well as connections that prevent longitudinal translation are located at the base of each plate girder, where the girder is supported by a concrete pier or abutment. These connections are labeled 'exp' and 'pinned' in figure 1. All subsequent discussions of the I-40 bridge will refer to the bridge carrying eastbound traffic, particularly the three eastern spans, which were the only ones tested.

3. Damage scenarios

The damage that was introduced was intended to simulate fatigue cracking that has been observed in plate-girder bridges. This type of cracking results from out-of-plane bending of the plate girder web and usually begins at welded attachments to the web such as the seats supporting the floor beams. Four levels of damage were introduced to the middle span of the north plate girder close to the seat supporting the floor beam at mid-span. Damage was introduced by making various torch cuts in the web and flange of the girder. It is acknowledged that the torch cuts produce simulated cracks too wide to open and close under the levels of excitation used in this investigation. Therefore, the nonlinear effects associated with a fatigue crack opening and closing could not be studied in this investigation.

The first level of damage, designated E-1, consisted of a two foot long, 10 mm wide (3/8 in wide) cut through the web centered at mid-height of the web. Next, this cut was continued to the bottom of the web to produce a second level of damage designated E-2. For the third level of damage, E-3, the flange was then cut halfway in from either side directly below the cut in the web. Finally, the flange was cut completely through for damage case E-4 leaving the top 4 ft of the web and the top flange to carry the load at this location. The various levels of damage are shown in figure 3. Photographs of these damage levels can be found in Farrar *et al* (1994).

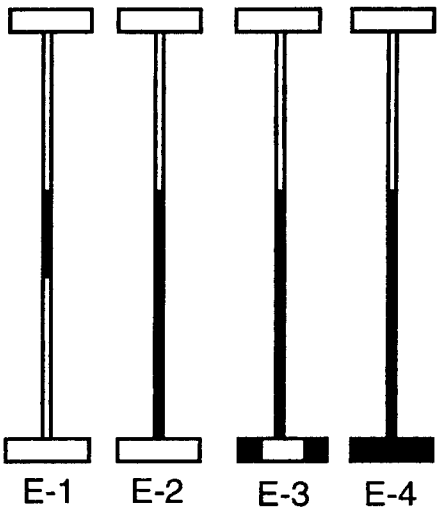

Figure 3. Portions of the north plate girder that were cut during the various damage scenarios.

4. Measurement of modal properties

The damage identification methods used in this study analyse mode shape data and, in some cases, the corresponding resonant frequencies. The experimental procedures used to obtain these data are described in this section. To obtain these data, a forced vibration test was conducted on the undamaged bridge. Eastbound traffic had been transferred to a new bridge just south of the one being tested. The westbound traffic continued on the original westbound bridge. Excitation from traffic on the adjacent bridges could be felt on the bridge being tested. Wind, although not measured, was not considered significant during these tests. Next, the four different levels of damage were introduced into the middle span of the north plate girder. Forced vibration tests similar to those done on the undamaged structure were repeated after each level of damage had been introduced. Weather conditions during these tests were similar to that reported for the undamaged test. Background sources of vibration were also similar. A detailed summary of the experimental procedures can be found in Farrar *et al* (1994).

4.1. Excitation

Engineers from Sandia National Laboratory (SNL) provided a hydraulic shaker that generated the measured force input. The SNL shaker consists of a 96.5 kN (21 700 lb) reaction mass supported by three air springs resting on top of drums filled with sand. A 9.79 kN (2200 lb) hydraulic actuator bolted under the center of the mass and anchored to the top of the bridge deck provided the input force to

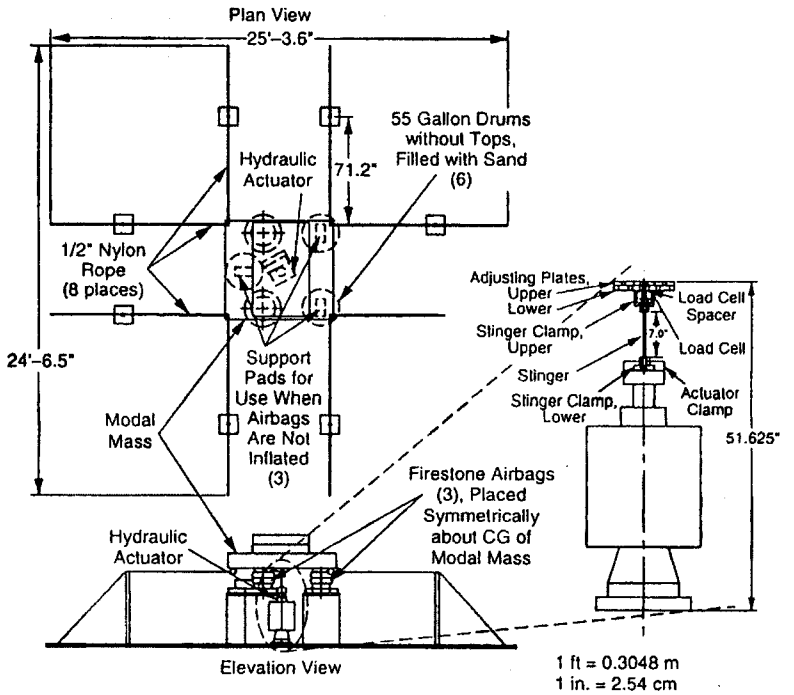

Figure 4. Shaker used for vibration testing of the I-40 bridge.

the bridge. Figure 4 shows a schematic diagram of the shaker. A random-signal generator was used to produce a 2000 lb peak-force uniform random signal over the frequency range of 2 to 12 Hz. An accelerometer mounted on the reaction mass was used to measure the force input to the bridge. This indirect force measurement gives the total force transferred to the bridge through the drums as well as the actuator. The shaker was located on the eastern-most span directly above the south plate girder and midway between the abutment and first pier. A more detailed summary of the Sandia shaker can be found in Mayes and Nusser (1994).

4.2. Data acquisition

The data acquisition system used in these tests consisted of a computer workstation that controlled 29 input modules and a signal processing module. The workstation was also the platform for a commercial data-acquisition/signal-analysis/modal-analysis software package. The input modules provided power to the accelerometers and performed analog-to-digital conversion of the accelerometer voltage–time histories. The signal-processing module performed the needed fast Fourier transform calculations. A 3500 watt AC generator was used to power this system in the field.

Two sets of integrated-circuit, piezoelectric accelerometers were used for the vibration measurements. A coarse set of measurements (SET1) was first made with twenty-six PCB model 336C accelerometers. These accelerometers were mounted in the vertical direction, on the inside web of the plate girder, at mid-height and at the axial locations shown in figure 5. These accelerometers had a nominal sensitivity of 1 V g^{-1}, a specified frequency range of 1–2000 Hz, and an amplitude range of ± 4 g. Thirty centimeter long (12 in long) 50 Ω cables attached to two conductor, PVC-jacketed 20-gauge cables ranging from 21.3 m to 88.9 m (70 ft to 291 ft) connected the accelerometers to the input modules.

Sampling parameters were specified that calculated the FRFs and cross-power spectra (CPS) from 30 averages of 32 s time windows discretized with 1024 samples yielding a frequency resolution of 0.031 25 Hz over a frequency range of 0–12.5 Hz. Hanning windows were applied to the time signals to minimize leakage, and AC coupling was specified to minimize DC offsets.

A more refined set of measurements (SET2) was made near the damage location. Eleven Endevco 7751-500 accelerometers with a nominal sensitivity of 500 mV g^{-1}, a frequency range of 0.4 to 1500 Hz, and an amplitude range of ± 10 g were placed in the global Y direction at a nominal spacing of 4.88 m (16 ft) along the mid-span of the north plated girder. All accelerometers were located at mid-height of the girder. The spacing of these accelerometers relative to the damage is shown in figure 6. The same data acquisition system, similar wiring and identical sampling parameters as those used with the coarse accelerometer set were again used with this refined set of accelerometers.

4.3. Modal parameter identification

Standard experimental modal analysis procedures were applied to data obtained from the SET1 accelerometers during the forced vibration tests to identify the modal parameters of the bridge in its damaged and undamaged condition. In this context experimental modal analysis refers to the procedure whereby a measured excitation

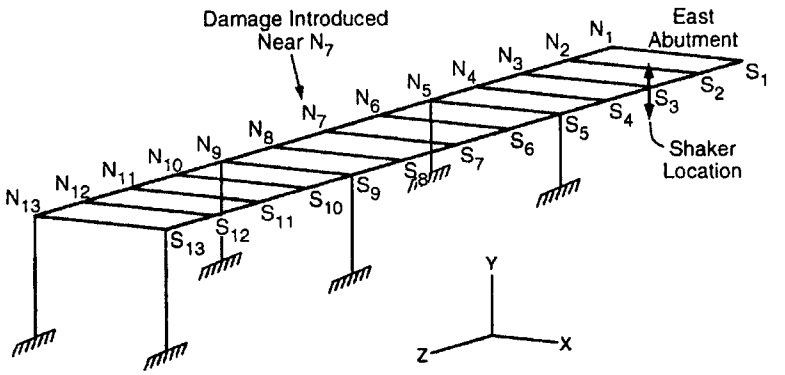

Figure 5. Locations of the coarse set of accelerometers.

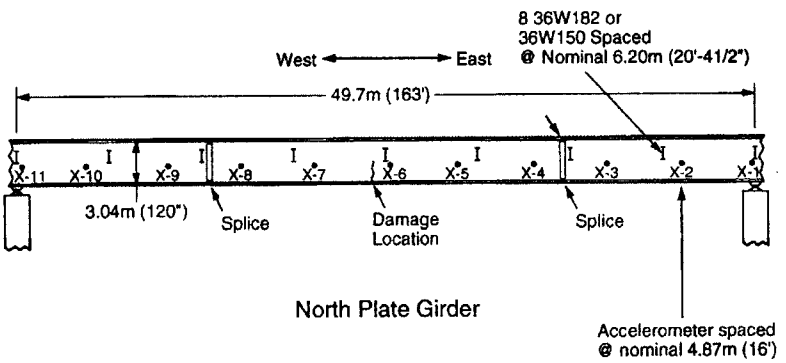

Figure 6. Locations of the refined set of accelerometers mounted on the middle span of the north plate girder.

(random, sine or impact force) is applied to a structure, and the structure's response (acceleration, velocity or displacement) is measured at discrete locations that are representative of the structure's motion. Both the excitation and the response time histories are transformed into the frequency domain in the form of FRFs. Modal parameters (resonant frequencies, mode shapes, modal damping) can be determined by curve-fitting a Laplace domain representation of the equations of motion to the measured frequency domain data (Ewins 1985). A rational-fraction polynomial, global, curve-fitting algorithm in a commercial modal analysis software package (Structural Measurements Systems 1987) was used to fit the analytical models to the measured FRF data and to extract resonant frequencies, mode shapes and modal damping values. Figure 7 shows the first six modes of the undamaged bridge identified from these data. By measuring the input force and the corresponding driving point acceleration, these mode shapes can be unit-mass normalized.

Immediately after the forced vibration tests with the SET1 accelerometers were complete, the random excitation tests were repeated using the refined SET2 accelerometers. For these tests the input was not monitored. Operating shapes were determined from amplitude and phase information contained in CPS of the various accelerometer readings relative to the accelerometer X-3 shown in figure 6. Determining operating shapes in this manner, as discussed by Bendat and Piersol (1980), simulates the methods that would have to be employed when the responses to ambient excitations are measured. For modes that are well spaced in frequency these operating shapes will closely approximate the mode shapes of the structure. However, without a measure of the input force these modes cannot be mass normalized.

5. Influence of damage on conventional modal properties

5.1. Changes in resonant frequencies and modal damping

Table 1 summarizes the resonant frequency and modal damping data obtained during each modal test of the undamaged and damaged bridge. No change in the dynamic properties can be observed until the final level of damage is introduced. At the final level of damage the resonant frequencies for the first two modes have dropped to values 7.6 and 4.4 percent less, respectively, than those measured during the undamaged tests. For modes where the damage was introduced near a node for that mode (modes 3 and 5) no significant changes in resonant frequencies can be observed.

5.2. Changes in mode shapes

A modal assurance criterion (MAC), sometimes referred to as a modal correlation coefficient (Ewins 1985), was

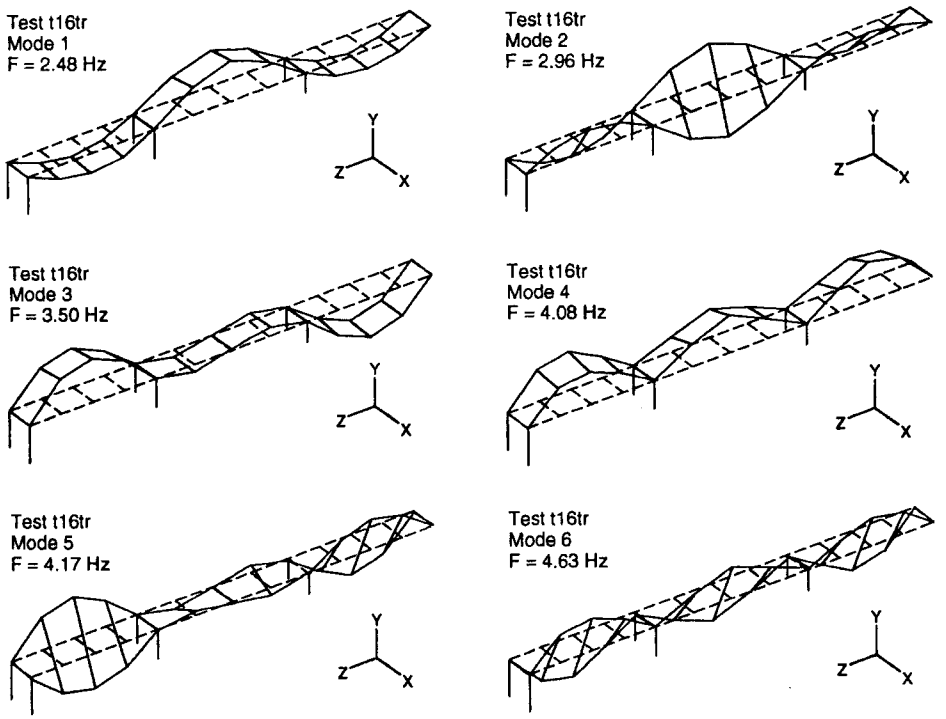

Figure 7. First six modes identified from forced vibration tests on the undamaged bridge.

Table 1. Resonant frequencies and modal damping values identified from undamaged and damaged forced vibration tests using SET1 accelerometers.

Test designation	Damage case	Mode 1 Freq. (Hz)/ damp. (%)	Mode 2 Freq. (Hz)/ damp. (%)	Mode 3 Freq. (Hz)/ damp. (%)	Mode 4 Freq. (Hz)/ damp. (%)	Mode 5 Freq. (Hz)/ damp. (%)	Mode 6 Freq. (Hz)/ damp. (%)
t16tr	Undamaged	2.48/ 1.06	2.96/ 1.29	3.50/ 1.52	4.08/ 1.10	4.17/ 0.86	4.63/ 0.92
t17tr	E-1 cut at center of web	2.52/ 1.20	3.00/ 0.80	3.57/ 0.87	4.12/ 1.00	4.21/ 1.04	4.69/ 0.90
t18tr	E-2 cut extended to bottom flange	2.52/ 1.33	2.99/ 0.82	3.52/ 0.95	4.09/ 0.85	4.19/ 0.65	4.66/ 0.84
t19tr	E-3 bottom flange cut half way	2.46/ 0.82	2.95/ 0.89	3.48/ 0.92	4.04/ 0.81	4.14/ 0.62	4.58/ 1.06
t22tr	E-4 bottom flange cut completely	2.30/ 1.60	2.84/ 0.66	3.49/ 0.80	3.99/ 0.80	4.15/ 0.71	4.52/ 1.06

calculated to quantify the correlation between mode shapes measured during different tests. The MAC makes use of the orthogonality properties of the mode shapes to compare two modes. If the modes are identical, a scalar value of one is calculated by the MAC. If the modes are orthogonal and dissimilar, a value of zero is calculated. The MAC that compares mode i and j has the form

$$\mathrm{MAC}(i,\ j) = \frac{|\sum_{k=1}^{n}(\phi_j)_k(\phi_i)_k^*|^2}{(\sum_{k=1}^{n}(\phi_j)_k(\phi_j)_k^*)(\sum_{k=1}^{n}(\phi_i)_k(\phi_i)_k^*)} \quad (1)$$

where $(\phi)_k$ is an element of the mode-shape vector and the asterisk denotes complex conjugate. Ewins points out that, in practice, correlated modes will yield a value greater than 0.9, and uncorrelated modes will yield a value less than 0.05.

Table 2 shows the MAC values that are calculated when mode shapes from tests t17tr (damage level E-1), t18tr (damage level E-2), t19tr (damage level E-3) and t22tr (damage level E-4) are compared to the modes measured on the undamaged forced vibration test, t16tr. The MAC values show no change in the mode shapes for the first

Table 2. Modal assurance criteria: undamaged and damaged forced vibration tests.

Mode	1	2	3	4	5	6
Undamaged (test t16tr) × first level of damage, E-1 (test t17tr)						
1	0.996	0.006	0.000	0.003	0.001	0.003
2	0.000	0.997	0.000	0.005	0.004	0.003
3	0.000	0.000	0.997	0.003	0.008	0.001
4	0.004	0.003	0.006	0.984	0.026	0.011
5	0.001	0.008	0.003	0.048	0.991	0.001
6	0.001	0.006	0.000	0.005	0.005	0.996
Undamaged (test t16tr) × second level of damage, E-2, (test t18tr)						
1	0.995	0.004	0.000	0.004	0.001	0.002
2	0.000	0.996	0.000	0.003	0.002	0.002
3	0.000	0.000	0.999	0.006	0.004	0.000
4	0.003	0.006	0.005	0.992	0.032	0.011
5	0.001	0.006	0.008	0.061	0.997	0.004
6	0.002	0.004	0.000	0.005	0.005	0.997
Undamaged (test t16tr) × third level of damage, E-3 (test t19tr)						
1	0.997	0.002	0.000	0.005	0.001	0.001
2	0.000	0.996	0.001	0.003	0.002	0.002
3	0.000	0.000	0.999	0.006	0.006	0.000
4	0.003	0.005	0.004	0.981	0.032	0.011
5	0.001	0.006	0.004	0.064	0.995	0.003
6	0.002	0.002	0.000	0.004	0.009	0.995
Undamaged (test t16tr) × fourth level of damage, E-4 (test t22tr)						
1	0.821	0.168	0.002	0.001	0.000	0.001
2	0.083	0.884	0.001	0.004	0.001	0.002
3	0.000	0.000	0.997	0.005	0.007	0.001
4	0.011	0.022	0.006	0.917	0.010	0.048
5	0.001	0.006	0.003	0.046	0.988	0.002
6	0.005	0.005	0.000	0.004	0.009	0.965

three stages of damage. When the final level of damage is introduced, significant drops in the MAC values for modes 1 and 2 are noticed. These two modes are shown in figure 8 and can be compared to similar modes identified for the undamaged bridge in figure 7. When the modes have a node near the damage location (modes 3 and 5), no significant reductions in the MAC values are observed, even for the final stage of damage. This result corresponds to the observed similarity in mode 3 shown in figures 7 and 8.

From the observed changes in modal parameters it is clear that damage can only be definitively identified after the final cut was made in the bridge. Prior to the final cut, one could not say that the changes observed were caused by damage or were within the repeatability of the tests. In two tests at increasing levels of damage (t17tr and t18tr) the resonant frequencies were actually found to increase slightly from that of the undamaged case. These slight increases in frequency were measured independently by other researchers studying this bridge at the same time (Farrar *et al* 1994) and are assumed to be caused by changing test conditions. The examination of changes in the basic modal properties (resonant frequencies and mode shapes) demonstrates the need for more sophisticated methods to examine modal data for indications of damage.

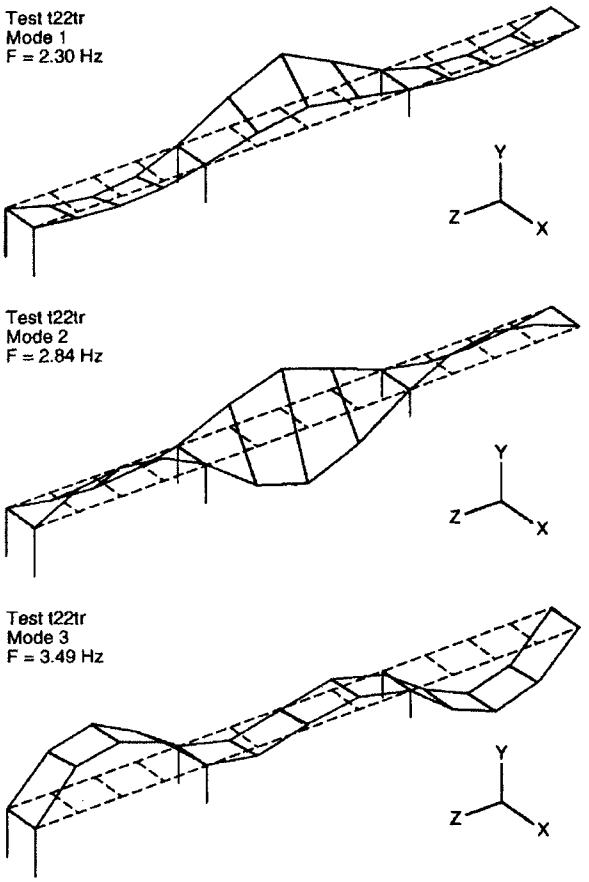

Figure 8. First three modes identified from forced vibration tests performed after the final level of damage had been introduced into the bridge.

Also, the need for statistical analysis of the data and quantification of the environmental effects on the measured modal properties is evident when one considers the small changes that are being examined. The topic of variability in bridge modal properties and statistical analysis of these properties is discussed in more detail in Farrar *et al* (1998), Doebling *et al* (1997).

6. Damage identification methods

The damage identification methods that were applied to the I-40 bridge data are briefly summarized below. Length limitations preclude a thorough development of these methods. For a more complete summary of these methods the reader is referred to the cited references or to Farrar and Jauregui (1996) where all the methods are discussed in detail.

6.1. Damage index method

The damage index method was developed by Stubbs and Kim (1994) to locate damage in structures given their characteristic mode shapes before and after damage. For a structure that can be represented as a beam, a damage index, β, is developed based on the change in strain energy stored in the structure when it deforms in its particular mode shape. For location j on the beam this change in the ith

mode strain energy is related to the changes in curvature of the mode at location j. The damage index for this location and this mode, β_{ij}, is defined as

$$\beta_{ij} = \frac{(\int_a^b [\psi_i^{*\prime\prime}(x)]^2\,dx + \int_0^L [\psi_i^{*\prime\prime}(x)]^2\,dx)}{(\int_a^b [\psi_i''(x)]^2\,dx + \int_0^L [\psi_i''(x)]^2\,dx)} \frac{\int_0^L [\psi_i''(x)]^2\,dx}{\int_0^L [\psi_i^{*\prime\prime}(x)]^2\,dx} \tag{2}$$

where $\psi_i''(x)$ and $\psi_i^{*\prime\prime}(x)$ are the second derivatives of the ith mode shape corresponding to the undamaged and damaged structures, respectively. L is the length of the beam. a and b are the limits of a segment of the beam where damage is being evaluated. When more than one mode is used, these authors define the damage index as the sum of damage indices from each mode. For mode shapes obtained from ambient data, the modes are normalized such that

$$\{\psi_n\}^{\mathrm{T}}[M]\{\psi_n\} = 1 \tag{3}$$

where $[M]$ is assumed to be the identity matrix.

To determine mode shape amplitudes at locations between sensors, the mode shapes are fit with a cubic polynomial. As shown in figure 9 for the refined set of accelerometers, the middle span of the north girder is divided into 160 0.305 m (1 ft) segments. Modal amplitudes are interpolated for each of the 161 nodes forming these segments. Similarly, for the coarse set of accelerometers the entire length of the north girder (all three spans) is divided into 210 0.610 m (2 ft) segments with mode shape interpolation yielding amplitudes at 211 node locations as shown in figure 9. Statistical methods are then used to examine changes in the damage index and associate these changes with possible damage locations. A normal distribution is fit to the damage indices, and values falling two or more standard deviations from the mean are assumed to be the most likely location of damage.

6.2. Mode shape curvature method

Pandey, Biswas and Samman (1991) assume that structural damage only affects the structure's stiffness matrix and its mass distribution. The pre- and post-damage mode shapes are first extracted from an experimental analysis. Curvature of the mode shapes for the beam in its undamaged and damaged conditions can then be estimated numerically from the displacement mode shapes with a central difference approximation or other means of differentiation. Given the before- and after-damage mode shapes, the authors consider a beam cross section at location x subjected to a bending moment $M(x)$. The curvature at location x along the length of the beam, $v''(x)$, is

$$v''(x) = M(x)/(EI) \tag{4}$$

where E is the modulus of elasticity and I the moment of inertia of the section.

From equation (4), it is evident that the curvature is inversely proportional to the flexural stiffness, EI. Thus, a reduction of stiffness associated with damage will, in turn, lead to an increase in curvature. Differences in the pre- and post-damage curvature mode shapes will, in theory, be largest in the damaged region. For multiple modes, the absolute values of change in curvature associated with each mode can be summed to yield a damage parameter for a particular location.

6.3. Change in flexibility method

Pandey and Biswas (1994) show that for the undamaged and damaged structure, the flexibility matrix, $[F]$, can be approximated from the unit-mass-normalized modal data as follows

$$[F] \approx \sum_{i=1}^{n} \frac{1}{\omega_i^2}\{\phi_i\}\{\phi_i\}^{\mathrm{T}} \tag{5}$$

and

$$[F]^* \approx \sum_{i=1}^{n} \frac{1}{\omega_i^{*2}}\{\phi_i\}^*\{\phi_i\}^{*\mathrm{T}} \tag{6}$$

where ω_i is the ith modal frequency, ϕ_i the ith unit-mass-normalized mode, n the number of measured modes and the asterisks signify properties of the damaged structure. Equations (5) and (6) are approximations because fewer modes are typically identified than the total numbers of measurement points or degrees of freedom. From the pre- and post-damage flexibility matrices, a measure of the flexibility change caused by the damage can be obtained from the difference of the respective matrices as

$$[\Delta F] = [F] - [F]^* \tag{7}$$

where $[\Delta F]$ represents the change in flexibility matrix. For each column of this matrix $\bar{\delta}_j$ is defined to be the absolute maximum value of the elements in that column. Hence,

$$\bar{\delta}_j = \max|\delta_{ij}| \qquad i = 1, \ldots, n \tag{8}$$

where δ_{ij} are elements of matrix $[\Delta F]$ and $\bar{\delta}_j$ is taken to be a measure of the flexibility change at each measurement location, j. The column of the flexibility matrix corresponding to the largest change is indicative of the degree of freedom where the damage is located.

6.4. Change in uniform load surface curvature

The coefficients of the ith column of the flexibility matrix represent the deflected shape assumed by the structure with a unit load applied at the ith degree of freedom. The sum of all columns of the flexibility matrix represents the deformed shape assumed by the structure if a unit load is applied at each degree of freedom, and this shape is referred to as the uniform load surface. Zhang and Aktan (1995) state that the change in curvature of the uniform load surface can be used to determine the location of damage. In terms of the curvature of the uniform load surface, F'', the curvature change at location l is evaluated as follows

$$\Delta F_i'' = |F_i^{*\prime\prime} - F_i''| \tag{9}$$

where $\Delta F''$ represents the absolute curvature change. The curvature of the uniform load surface can be obtained with a central difference operator as suggested by these authors.

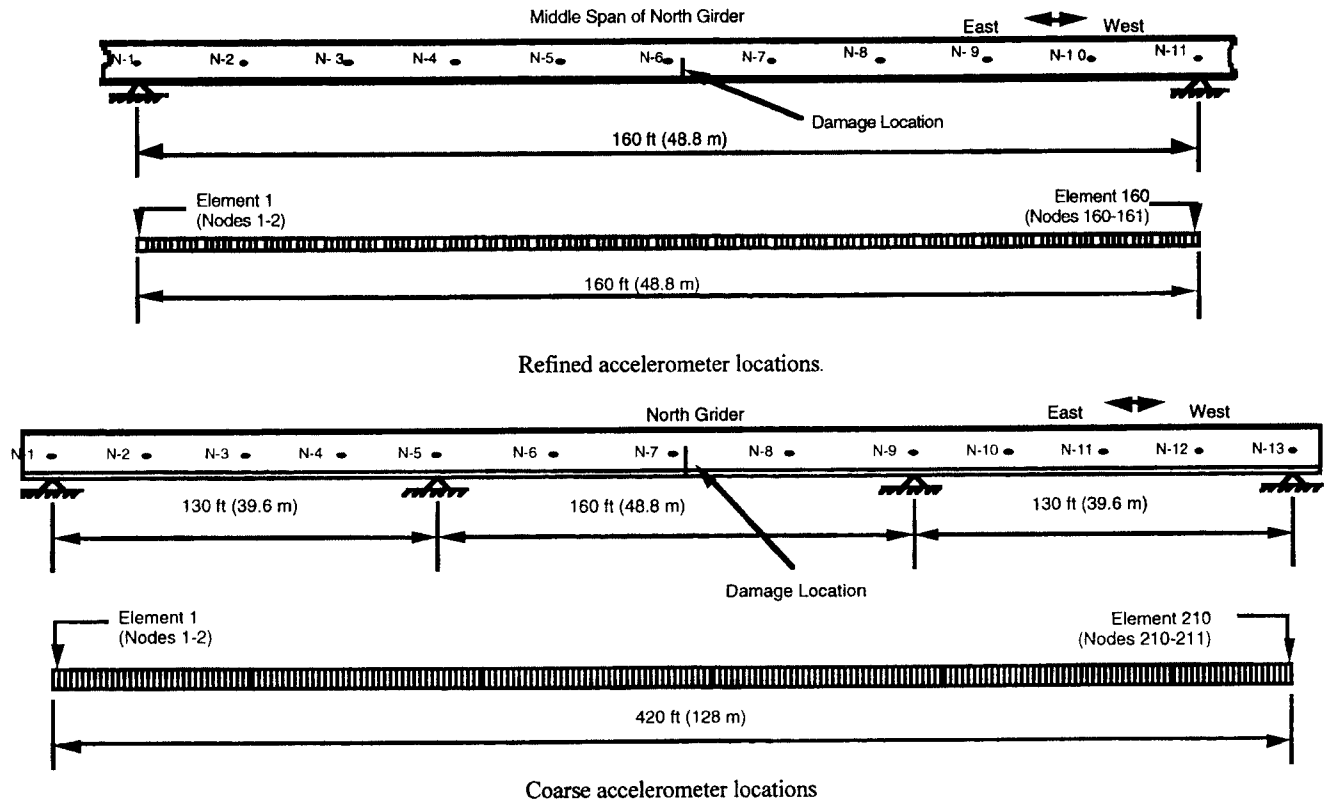

Figure 9. Discretization of the north plate girder used to interpolate mode shape amplitudes.

6.5. Change in stiffness method

Zimmerman and Kaouk (1994) have developed a damage detection method based on changes in the stiffness matrix that is derived from measured modal data. The eigenvalue problem of an undamaged, undamped structure is

$$\left(\lambda_i[M]+[K]\right)\{\psi_i\} = \{0\}. \tag{10}$$

The eigenvalue problem of the damaged structure is formulated by first replacing the pre-damaged eigenvectors and eigenvalues with a set of post-damaged modal parameters and, second, subtracting the perturbations in the mass and stiffness matrices caused by damage from the original matrices. Letting ΔM_d and ΔK_d represent the perturbations to the original mass and stiffness matrices, the eigenvalue equation becomes

$$\left[\lambda_i^*[M-\Delta M_d]+[K-\Delta K_d]\right]\{\psi_i\}^* = \{0\}. \tag{11}$$

Two forms of a damage vector, $\{D_i\}$, for the ith mode are then obtained by separating the terms containing the original matrices from those containing the perturbation matrices. Hence,

$$\{D_i\} = \left(\lambda_i^*[M]+[K]\right)\{\psi_i\}^* = \left(\lambda_i^*[\Delta M_d]+[\Delta K_d]\right)\{\psi_i\}^*. \tag{12}$$

To simplify the investigation, damage is considered to alter only the stiffness of the structure (i.e. $[\Delta M_d] = [0]$). Therefore, the damage vector reduces to

$$\{D_i\} = [\Delta K_d]\{\psi_i\}^*. \tag{13}$$

In a similar manner as the modal-based flexibility matrices previously defined, the stiffness matrices, before and after damage, can be approximated from incomplete mass-normalized modal data as

$$[K] \approx \sum_{i=1}^{n} \omega_i^2 \phi_i \phi_i^{\mathrm{T}} \tag{14}$$

and

$$[K]^* \approx \sum_{i=1}^{n} \omega_i^{*2} \phi_i^* \phi_i^{*\mathrm{T}}. \tag{15}$$

Equation (15) is subtracted from equation (14) to obtain $[\Delta K_d]$. This matrix is multiplied by the ith damaged mode shape vector to obtain the ith damage vector as shown in equation (13). A scaling procedure discussed by Zimmerman and Kaouk was used to avoid spurious readings at stiff locations near supports where the signal-to-noise ratio of the measured responses is lower.

7. Modifications made to the methods to facilitate direct comparisons

The primary modification made to these methods was the adaptation of the cubic polynomial interpolation scheme to approximate mode shape amplitudes at locations between sensors as suggested by Stubbs and Kim (1994). This interpolation effectively introduces artificial degrees of freedom into the experimental measurements. Also, the cubic polynomial can be directly differentiated to obtain the needed mode shape curvatures thus avoiding the

finite difference scheme for evaluating the mode shape derivatives suggested by some authors. If damage can be located to within the resolution of the interpolated mode shape amplitudes, a level II damage diagnosis was considered successful.

Two of the damage detection methods require only consistently normalized mode shapes, namely the damage index method and the mode shape curvature method. The change in flexibility method, the change in uniform load surface curvature method and the change in stiffness method require the resonant frequency for each mode and mass-normalized mode shape vectors. When the methods that require unit-mass normalized mode shapes were applied to the mode shape data obtained with the SET2 instruments, the mass along the length of the beam was considered constant and these mode shapes were normalized using equation (3). Because these damage detection methods are only concerned with changes in flexibility or stiffness matrices rather than their absolute values, it was assumed that this method of mode shape normalization would not introduce significant errors into the damage detection process.

8. Application of damage identification methods to experimental data

Figures 10 through 19 show the results from the different damage identification methods when they are applied to data from damage cases E-1 and E-4 obtained with the SET2 and SET1 instruments. For the SET2 instruments the actual damage location was between nodes 82 and 83. For the SET1 instruments the actual damage location was between nodes 106 and 107. Also shown for the data from the SET1 instruments (except for the change in uniform load surface method) is the influence of the number of modes on the damage detection process. Plots of the damage indicators for the intermediate damage cases (E-2 and E-3) can be found in Farrar and Jauregui (1996). Tables 3 and 4 summarize the results from applying the five damage detection algorithms to the experimental modal data from the SET1 and SET2 instruments, respectively. In this study, the damage index method was found to have performed the best.

The change in stiffness method improved when applied to the modal data from the coarse set of accelerometers. Significant improvements to this method were also shown when only the first two modes were used instead of all six as shown in table 4. Using the refined measurements, only the final damage case (E-4) was detected with this method, whereas all damage cases were detected from the SET2 modal data. One possible explanation for this observation is that to calculate the modal-based stiffness matrix, unit-mass-normalized mode shapes are needed, and only modes obtained from the SET1 instruments are unit-mass-normalized modes.

9. Summary and conclusions

The application of five linear damage identification methods using experimental modal data gathered from the I-40 bridge over the Rio Grande in Albuquerque, NM has been reported. In this study linear damage identification implies that linear dynamic models were used to model the structure both before and after damage. The nature of the damage applied to the I-40 bridge is such that the linear damage models are applicable to these damage scenarios. This study provides a direct comparison of various damage identification algorithms when applied to a standard problem. The authors are not aware of other such comparisons that have been reported in the technical literature.

Examination of results from the experimental modal analyses verify other investigators' findings that standard modal properties such as resonant frequencies and mode shapes are poor indicators of damage. The more sophisticated damage detection methods investigated herein showed improved abilities to detect and locate the damage. In general, all methods investigated in this study identified

Table 3. Summary of damage detection results using experimental modal data from coarse set of accelerometers (SET1).

	E-1	E-2	E-3	E-4
Damage index method	**	**	**	*
Mode shape curvature method	**	*	**	*
Change in flexibility method	o	o	**	*
Change in uniform load surface curvature method	o	o	o	*
Change in stiffness method	**	**	**	*

* Damage located; ** damage located using only two modes; o damage not located.

Table 4. Summary of damage detection results using experimental modal data from refined set of accelerometers (SET2).

	E-1	E-2	E-3	E-4
Damage index method	•	•	•	•
Mode shape curvature method	•••	••	•	•
Change in flexibility method	o	o	o	•
Change in uniform load surface curvature method	o	•••	•	•
Change in stiffness method	o	o	o	•

• Damage located; •• damage narrowed down to two locations; ••• damage narrowed down to three locations; o damage not located.

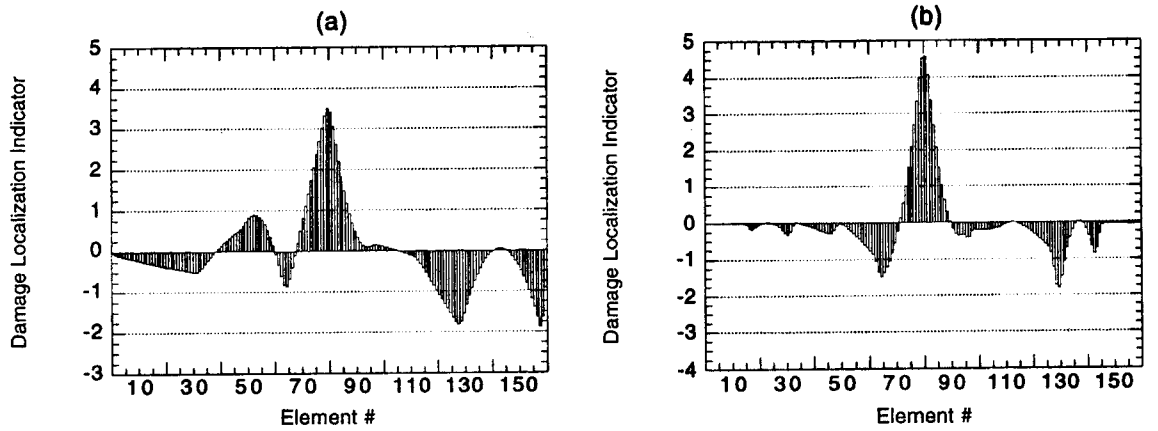

Figure 10. Results of damage index method applied to the SET2 modal data from damage scenario E-1 (a) and E-4 (b).

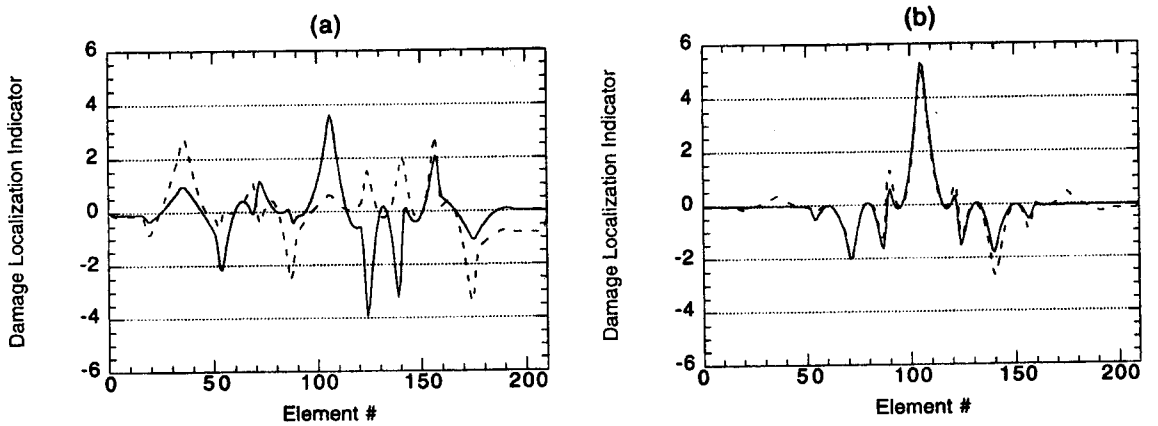

Figure 11. Results of damage index method applied to the SET1 modal data from damage scenario E-1 (a) and E-4 (b): ——, two modes; - - - -, six modes.

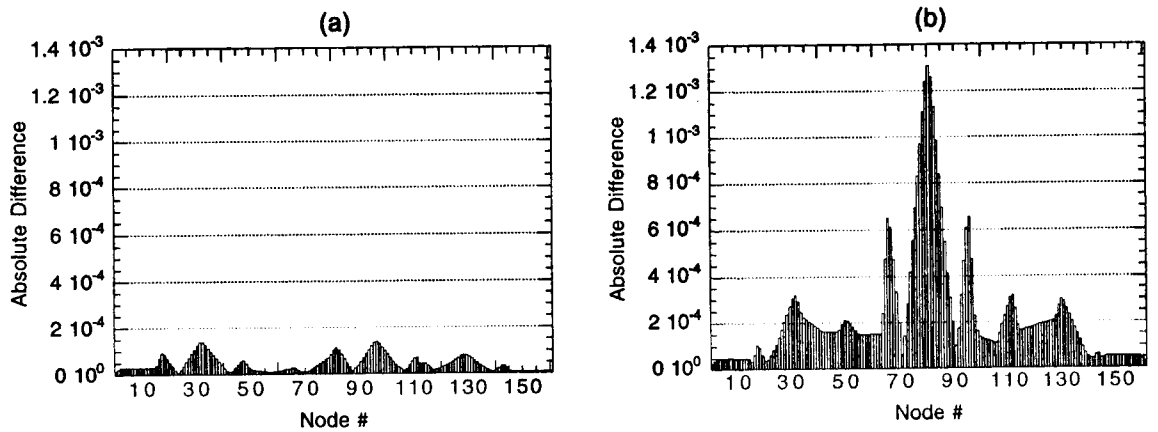

Figure 12. Absolute difference in mode shape curvatures between the undamaged and damaged bridge for damage case E-1 (a) and E-4 (b) computed using the SET2 modal data.

the damage location correctly for the most severe damage case: a cut through more than half the web and completely through the bottom flange. However, for several of these methods, if they had been applied blindly, it would be difficult to tell whether damage had not also occurred at locations other than the actual one. The methods were inconsistent and did not clearly identify the damage location when they were applied to the less severe damage cases. Results of this study show that the damage index method performed the best when the entire set of tests are considered. This performance is attributed to the methods of normalizing changes in the damage parameters relative

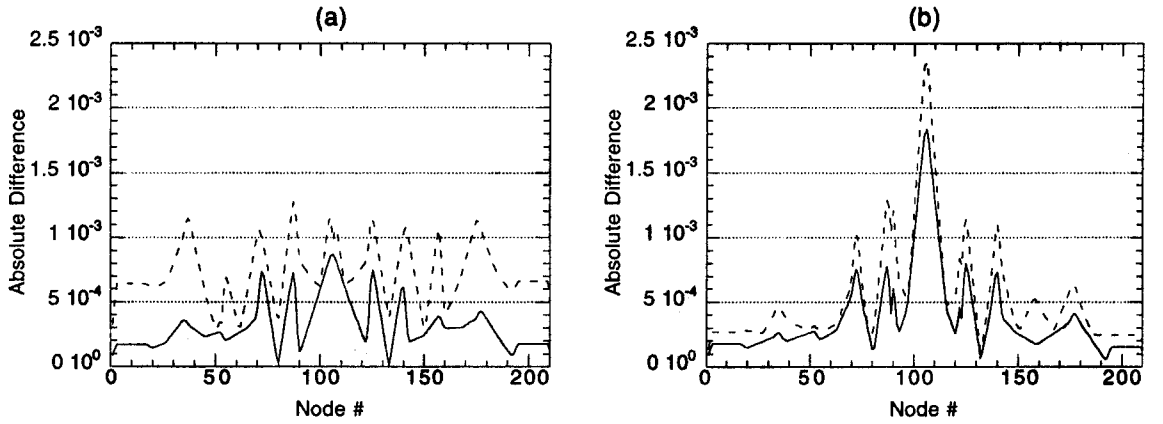

Figure 13. Absolute difference in mode shape curvatures between the undamaged and damaged bridge for damage case E-1 (a) and E-4 (b) computed using the SET1 modal data: ——, two modes; - - - -, six modes.

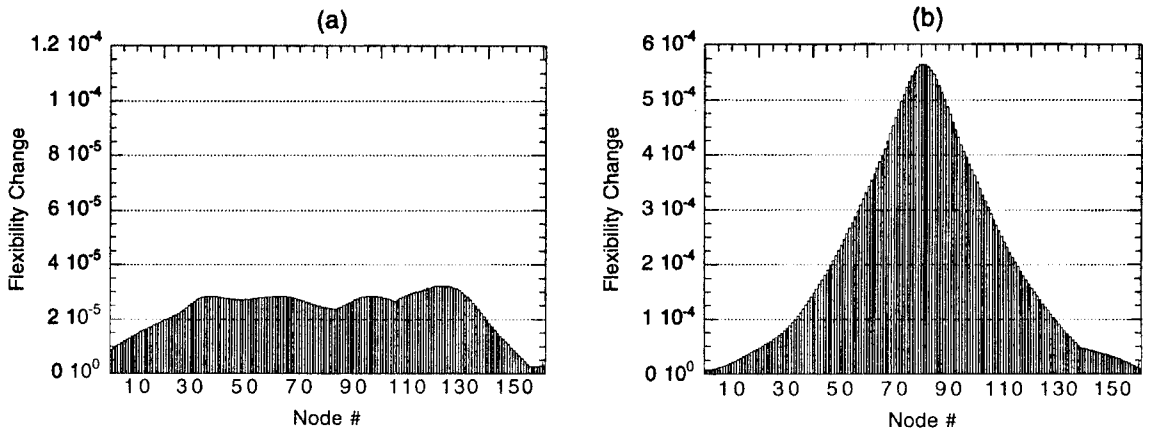

Figure 14. Results of change in flexibility method applied to the SET2 modal data from damage scenario E-1 (a) and E-4 (b).

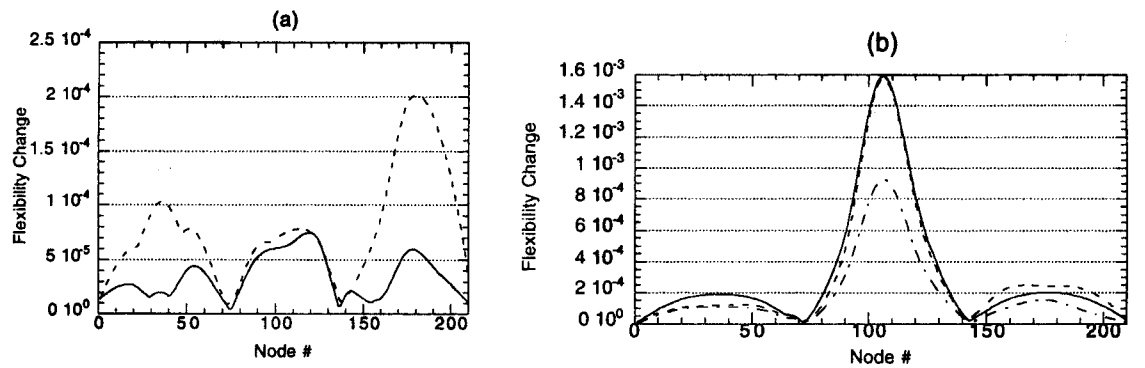

Figure 15. Results of change in flexibility method applied to the SET1 modal data from damage scenario E-1 (a) and E-4 (b): ——, two modes; - - - -, six modes.

to the undamaged case. Also, the damage index method works with mode shape data that do not have to be unit-mass normalized. This feature is desirable when an on-line monitoring system that uses ambient traffic excitation is being considered.

Another observation from this study, which the authors feel is important, is that the damage index method is the only method tested that has a specific criterion for determining whether damage has occurred at a particular location. The other methods only look for the largest change in a particular parameter and it is ambiguous at times to determine whether these changes indicate damage at more than one location. This ambiguity is illustrated in figures 12 and 16 where, in a blind test, it would be difficult to tell whether damage has occurred at one or three locations. This point is further studied with numerical models in the accompanying paper (Farrar and Jauregui 1998). The probabilistic method employed by

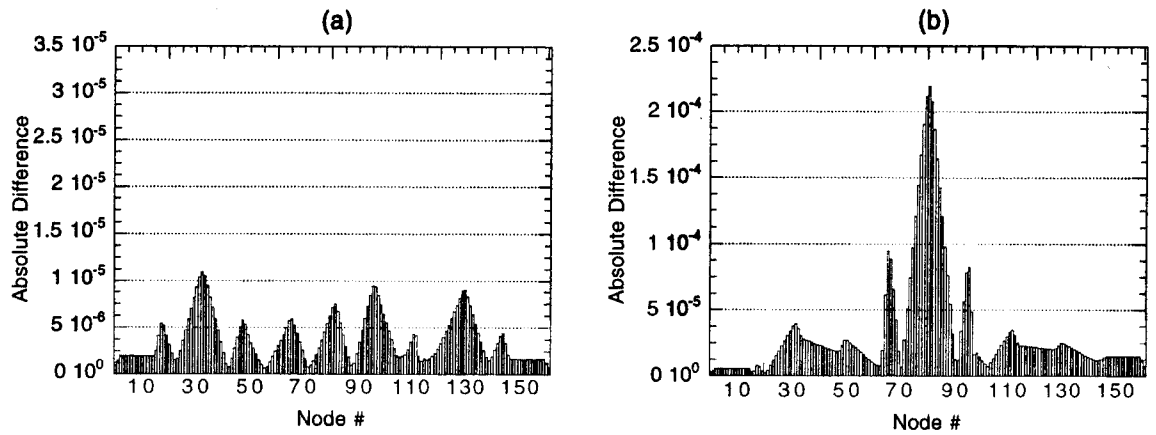

Figure 16. Results of change in uniform load surface curvature method applied to the SET2 modal data from damage scenario E-1 (a) and E-4 (b).

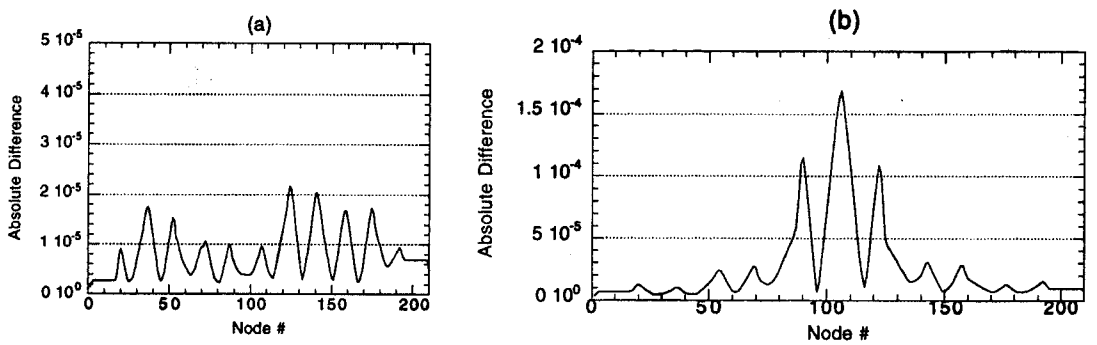

Figure 17. Results of change in uniform load surface curvature method applied to the SET1 modal data from damage scenario E-1 (a) and E-4 (b).

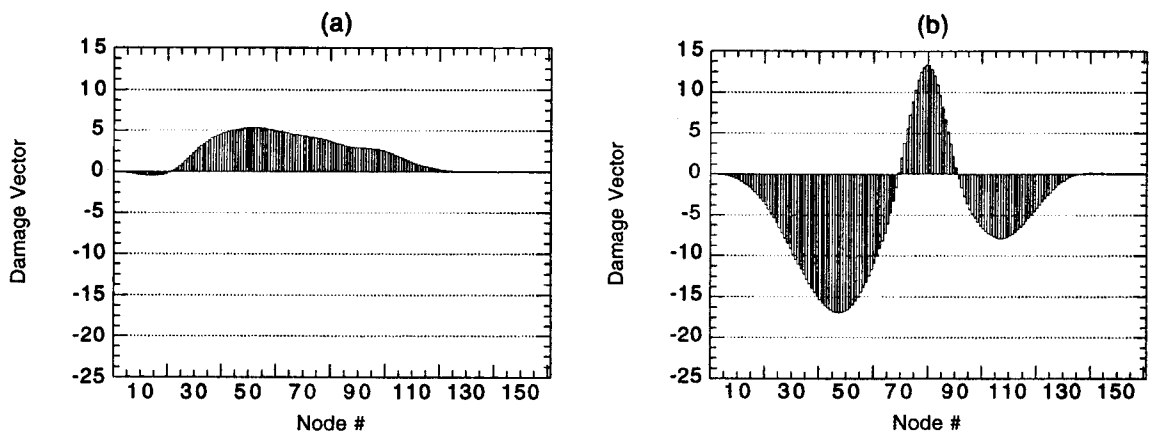

Figure 18. Results of change in stiffness method applied to the SET2 modal data from damage scenario E-1 (a) and E-4 (b).

the damage index method to determine whether changes in the monitored parameter were indicative of damage could be implemented with the other four methods that were investigated as well.

For the methods that are based on the change in the flexibility or stiffness matrix derived from modal properties, further studies are needed to assess the effects of assuming an identity mass matrix when normalizing the mode shapes obtained from ambient tests. Because the change in stiffness method performed significantly better with data from tests where the mode shapes were unit-mass normalized, it is possible that normalizing the modes with this assumed matrix was introducing errors into the estimates of the flexibility and stiffness matrix.

The authors acknowledge that the results reported in this study are valid only for the structure tested and are based on a limited number of data that could be collected during the allotted testing time. A large data

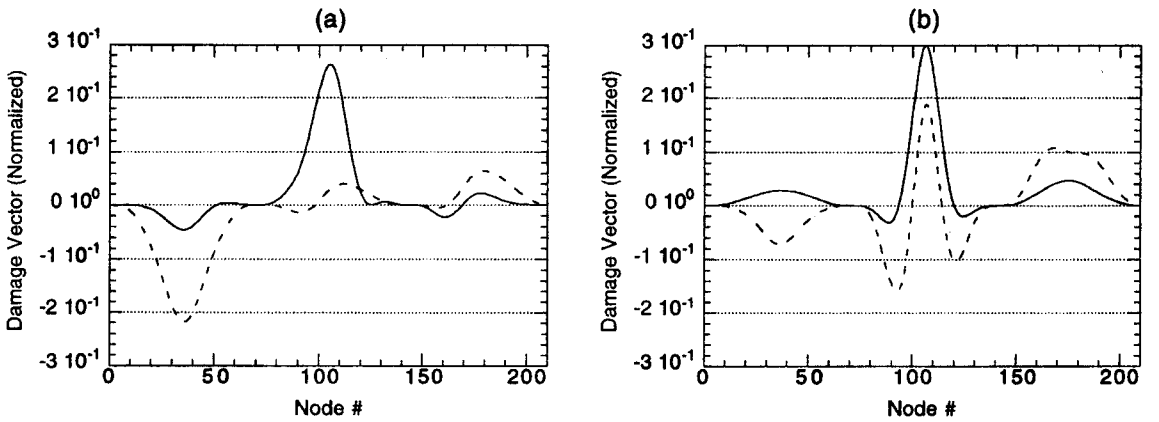

Figure 19. Results of change in stiffness method applied to the SET1 modal data from damage scenario E-1 (a) and E-4 (b): ——, two modes; - - - -, six modes.

base of various structure types and damage scenarios must be investigated before general statements regarding the relative merits of the various damage identification methods can be stated absolutely. Also, variation in sensor distribution, excitation location, and the damage location could potentially influence the outcome of such a study. Safety concerns regarding the removal of the shaker after damage and the time necessary to relocate the shaker precluded any studies with the excitation at different locations. Time and budget constraints on the testing preclude the repair of the damage and the relocation of the damage. Finally, the sensor locations were not altered because it was assumed that these locations represent a logical layout of the sensors if a general damage monitoring system was put into place without prior knowledge of the damage location and with some reasonable economic constraints on the instrumentation scheme.

Based on further analysis and observations related to the I-40 bridge tests, subsequent tests on another bridge and a review of the technical literature related to bridge testing, there are several things that should have been done during these tests to improve the confidence in the damage ID results. These improvements in the testing procedure are listed below:

(1) Perform a thorough pre-test visual inspection and continue to perform visual inspections as weather conditions change. Weather conditions can have a significant effect on the boundary conditions of the bridge.

(2) Perform linearity and reciprocity checks. The system identification portion of the experimental modal analysis procedure typically relies on the assumption that the structure is linear and will exhibit reciprocity. Linearity can be checked, to some degree, by exciting the structure at different levels and overlaying the measured FRFs for a particular point. Ideally, with the thought of an on-line monitoring system in mind, these different excitation levels would span the range of loading observed during ambient traffic vibration measurements. Also, a change in the linearity properties can in itself indicate damage.

In addition to the assumption of linearity, the system identification portion of the experimental modal analysis typically relies on the assumption that the structure will exhibit reciprocity. Performing a reciprocity check is much more involved when a large shaker is being used because of the setup time involved in relocating the shaker. Also, to check the reciprocity of the structure alone, one must relocate the accelerometers and cables as well as the shaker. Without moving the instrumentation, the reciprocity check will involve reciprocity of the measurement electronics as well as that of the structure.

(3) Perform as many environmental and testing procedure sensitivity studies as possible. Sensitivity of modal test results to environmental conditions and test procedures such as changes in temperature, traffic loading, wind, excitation method etc should be quantified to the extent possible. Subsequent tests (after the potential damage has occurred) should be performed under similar environmental conditions using similar test procedures, if possible. Also, a baseline noise measurement should be made for the data acquisition system.

Three areas of research currently being pursued by the authors were suggested by the results reported in this study. First, there is a need to develop statistical analysis procedures based on Monte Carlo methods or bootstrap methods that can establish confidence limits on identified modal parameters. Then the changes in these parameters, or quantities derived from these parameters such as the damage index or the modal-based flexibility, can be attributed to damage rather than the repeatability of the experiment. Second, it appears that only using the modes that are most influenced by damage can enhance the damage detection process. Therefore, the authors are currently studying methods to screen and select the modes to be used in the damage detection process. Finally, a more basic form of the study reported herein, which performs the same comparative study of vibration-based damage identification methods on simple structural elements, is currently being pursued. This new study will potentially help identify the basic differences in the various methods' ability to accurately identify and located damage.

The authors acknowledge that the application of these damage detection methods was simplified because of the beam-like behavior of the damaged member and because the location of the damage was known prior to the

application of these methods. Clearly, more tests on actual structures such as the one reported in this study are needed before these methods can be applied with sufficient confidence to warrant the field deployment of remote monitoring systems. The numerical studies reported in the accompanying paper attempt to provide more information on the relative merits of these various damage detection methods. Finally, it should be noted that this comparative study has been extended to include finite element model updating methods of damage detection as reported by Simmermacher *et al* (1995).

Acknowledgments

The authors would like to acknowledge the cooperation and teamwork that was exhibited by all parties involved in these tests including engineers from Sandia National Laboratory; faculty, technicians and students from New Mexico State University; numerous people at the New Mexico State Highway and Transportation Department and the staff at the Alliance for Transportation Research.

References

Alampalli S, Fu G and Dillon E W 1995 On the use of measured vibration for detecting bridge damage *Proc. 14th Int. Modal Analysis Conf.* vol 1, pp 125–37

Bendat J S and Piersol A G 1980 *Engineering Applications of Correlation and Spectral Analysis* (New York: Wiley)

Biswas M, Pandey A and Bluni S 1994 Modified chain-code computer vision techniques for interrogation of vibration signatures for structural fault detection *J. Sound Vib.* **175** 89–104

Biswas M, Pandey A K and Samman M M 1990 Diagnostic experimental spectral/modal analysis of a highway bridge *Int. J. Anal. Exp. Modal Anal.* **5** 33–42

Doebling S W *et al* 1996 Damage identification in structures and mechanical systems based on changes in their vibration characteristics: a detailed literature review *Los Alamos National Laboratory Report* LA-13070-MS

Doebling S W, Farrar C R and Goodman R 1997 Effects of measurement statistics on the detection of damage in the Alamosa Canyon Bridge *Proc. 15th Int. Modal Analysis Conf. (Orlando, FL)*

Ewins D J 1985 *Modal Testing: Theory and Practice* (New York: Wiley)

Farrar C R *et al* 1994 Dynamic characterization and damage detection in the I-40 bridge over the Rio Grande *Los Alamos National Laboratory Report* LA-12767-MS

Farrar C R, Doebling S W, Cornwell P J and Straser E G 1997 Variability of modal parameters measured on the Alamosa Canyon Bridge *Proc. 15th Int. Modal Analysis Conf. (Orlando, FL)*

Farrar C R and Jauregui D 1996 Damage detection algorithms applied to experimental and numerical modal data from the I-40 bridge *Los Alamos National Laboratory Report* LA-13074-MS

——1998 Comparative study of damage identification algorithms applied to a bridge: II. Numerical study *Smart Mater. Struct.* **7** 720–31

Jain B K 1991 Diagnostics through experimental vibration signature analysis of prestressed concrete bridges *Int. Symp. on Fracture in Steel and Concrete Structures* pp 1123–36

Kato M and Shimada S 1986 Vibration of PC bridge during failure process *ASCE J. Struct. Eng.* **112** 1692–703

Kim J-T and Stubbs N 1993 Assessment of the relative impact of model uncertainty on the accuracy of global nondestructive damage detection in structures *Report prepared for New Mexico State University*

Kobayashi A S (ed) 1987 *Handbook on Experimental Mechanics* (Englewood Cliffs, NJ: Society for Experimental Mechanics–Prentice-Hall)

Kong F, Liang Z and Lee G C 1996 Bridge damage identification through ambient vibration signature *Proc. 14th Int. Modal Analysis Conf. (Dearborn, MI)* vol 1, pp 706–12

Law S S, Waldron P and Taylor C 1992 Damage detection of a reinforced concrete bridge deck using frequency response function *Proc. 11th Int. Modal Analysis Conf.* vol 2, pp 772–8

Liang Z, Tong M and Lee G C 1995 Modal energy measurements of a long steel bridge *Proc. 13th Int. Modal Analysis Conf.* vol 1, pp 226–32

Mayes R L 1995 An experimental algorithm for detecting damage applied to the I-40 bridge over the Rio Grande *Proc. 13th Int. Modal Analysis Conf.* vol 1, pp 219–25

Mayes R L and Nusser M A 1994 The Interstate-40 Bridge Shaker Project *Sandia National Laboratory Report* SAND94-0228

Mazurek D F and DeWolf J T 1990 Experimental study of bridge monitoring technique *ASCE J. Struct. Eng.* **116** 2532–49

Pandey A K and Biswas M 1994 Damage detection in structures using changes in flexibility *J. Sound Vib.* **169** 3–17

Pandey A K, Biswas M and Samman M M 1991 Damage detection from changes in curvature mode shapes *J. Sound Vib.* **145** 321–32

Raghavendrachar M and Aktan A E 1992 Flexibility by multireference impact testing for bridge diagnostics *ASCE J. Struct. Eng.* **118** 2186–203

Rytter A 1993 Vibration based inspection of civil engineering structures *Doctoral Dissertation* Department of Building Technology and Structural Engineering, University of Aalborg

Salane H J, Baldwin J W and Duffield R C 1981 Dynamics approach for monitoring bridge deterioration *Transportation Res. Record* **832** 21–8

Salawu O S 1995 Non-destructive assessment of structures using the Integrity Index method applied to a concrete highway bridge *Insight* **36** 875–8

Salawu O S and Williams C 1995 Review of full-scale dynamic testing of bridge structures *Eng. Struct.* **17** 113–21

Samman M M and Biswas M 1994 Vibration testing for nondestructive evaluation of bridges II. Results *ASCE J. Struct. Eng.* **120** 290–306

Samman M M, Biswas M and Pandey A K 1991 Employing pattern recognition for detecting cracks in a bridge model *Int. J. Anal. Exp. Modal Anal.* **6** 35–44

Shirole A M and Holt R C 1991 Planning for a comprehensive bridge safety assurance program *Transportation Res. Record* **1290** 39–50

Simmermacher T, Zimmerman D C, Mayes R L, Reese G M and James G H 1995 The effects of finite element grid density on model correlation and damage detection of a bridge *Proc. 36th AIAA/ASME/ASCE/AHS/ASC Structures, Structural Dynamics, and Materials Conf.*

Spyrakos C, Chen H L, Stephens J and Govidaraj V 1990 Evaluating structural deterioration using dynamic response characterization *Proc. Intelligent Structures* (Elsevier) pp 137–54

Structural Measurements Systems 1987 *Modal* 3.0 (San Jose, CA: Structural Measurements Systems)

Stubbs N and Kim J-T 1994 Field verification of a nondestructive damage localization and severity estimation algorithm *Texas A&M University Report prepared for New Mexico State University*

Stubbs N, Kim J-T and Farrar C R 1995 Field verification of a

nondestructive damage localization and severity estimation algorithm *Proc. 13th Int. Modal Analysis Conf.* vol 1, pp 210–8

Tang J P and Leu K-M 1991 Vibration tests and damage detection of P/C bridges *J. Chin. Inst. Eng.* **14** 531–6

Toksoy T and Aktan A E 1994 Bridge-condition assessment by modal flexibility *Exp. Mech.* 271–8

Turner J D and Pretlove A J 1988 A study of the spectrum of traffic-induced bridge vibration *J. Sound Vib.* **122** 31–42

White K R, Minor J and Derucher K N 1992 *Bridge Maintenance, Inspection and Evaluation* (New York: Dekker)

Zhang Z and Aktan A E 1995 The damage indices for the constructed facilities *Proc. 13th Int. Modal Analysis Conf.* vol 2, pp 1520–9

Zimmerman D C and Kaouk M 1994 Structural damage detection using a minimum rank update theory *J. Vib. Acoust.* **116** 222–31